Non-Destructive Assay of Spent Nuclear Fuel Using Gamma-Ray Mirrors as a Narrow Band Pass Filter

K.P. Ziock,[1] M.-A. Descalle,[2] J. Ruz,[2,3] K. Schmitt,[1] J.M. Harp[1]

1. Oak Ridge National Laboratory (ORNL), Oak Ridge, TN[1]

2. Lawrence Livermore National Laboratory, Livermore, CA

3. Now with, Center for Astroparticles and High Energy Physics (CAPA), Universidad de Zaragoza, Zaragoza, Spain

Abstract

As a material of concern for proliferation, we are interested in measuring the Pu content of spent fuel by comparing the ratio of fluorescence K-shell emissions from U and Pu. With emission stimulated by higher energy background, these lines have the advantage that they remain visible above the copious background. However, the low-intensity Pu Kα1 line (103.7 keV) sits where the background is highest, creating detector deadtime and resolution issues while requiring very high spectral resolution to separate it from the adjacent 105.3-keV line from ^{155}Eu. Unfortunately, around 100 keV, only tight collimation can be used to control the direct flux reaching the detector, so the low intensity of the Pu line means long integration times are needed.

We are exploring high-efficiency, gamma-ray mirrors as defined band-pass filters to deflect the K-shell spectral region (94 to 120 keV) onto a point-contact, high-purity germanium detector shielded from the fuel's direct flux, completely removing rate issues. Such mirrors are manufactured by depositing hundreds of alternating layers of SiC and WC onto flat surfaces. By varying the layer spacing throughout the depth of the coating, reflectivity can be tuned to cover an angle/energy range suitable to the measurement. Several mirrors have been fabricated with over 400 aperiodic bi-layer pairs providing a ~0.2^0 reflection with a flattop response over a bandpass of 94 to 110 keV. The mirrors were recently tested at the ORNL Irradiated Fuel Examination Laboratory, providing almost an order of magnitude flux increase over earlier results obtained with a mirror made of a periodic multilayer, with a single bi-layer thickness. A two-mirror stacked system yielded statistically significant results for the Pu content from several ~ 7-cm-long locations on LWR spent fuel pins with different burn-up values. This paper presents the overall system and the results of those measurements.

Introduction

During irradiation ^{238}U present in low enriched uranium begins to transmute to ^{239}Pu. In a light water reactor, the rate of Pu production varies with local neutron flux, starting uranium isotopics used in different parts of a fuel rod, and irradiation history. The ability to non-destructively measure Pu concentration in fuel is useful in benchmarking neutronics simulations and may be useful in providing additional information for nuclear material accountability (NMC&A) purposes. In particular, one is concerned with

---

reprocessing when safeguarded fuel changes from item accountancy to accountancy by the amount of material actually present (determined by destructive assay). Invariably, the Pu content determined from the fuel history and burn-up codes does not yield the same content as a destructive analysis, leading to receiver-operator differences that must be reconciled. Spent fuel is also finding its way to permanent underground disposal, and as such facilities come on line, there is a desire to fully understand what is being disposed of before the NMC&A books are closed.

Obtaining a direct measure of the Pu:U ratio in spent fuel is desirable for all of these reasons, however quickly obtaining accurate results with NDA is complicated by the high radiation emission rates of the materials, and the relatively low Pu content (~1%) present in the fuel. The prominent nuclear lines that might be used for spectral analysis of isotopically pure materials (186 keV for ^{235}U, 129 keV, 375 keV, and 414 keV for ^{239}Pu) are invariably swamped by the Compton continuum from the radiation produced by the various fission daughters present in the spent fuel. However, the emission of K-shell x-rays from both materials is fed by fluorescence as the atoms are continually bombarded by the high-energy radiation environment, so that they should be readily visible. This is true for the U K-shell lines that are a prominent feature of spent fuel spectra (Fig. 1). However, with its low abundance, the Pu emissions are much weaker and at 103.7 keV the Pu Kα1 line is only 1.6 keV from the 105.3-keV nuclear line emitted by the ^{155}Eu fission product that is of comparable intensity. Consequently, to separate the lines for quantitative spectral analysis requires a high-quality, high-purity germanium (HPGe) spectrum and invariably that means low rates with relatively long event processing times. The possibility of the measurement has been demonstrated [1], but the requisite tight collimation needed to maintain spectral resolution, meant impractically long measurement times.

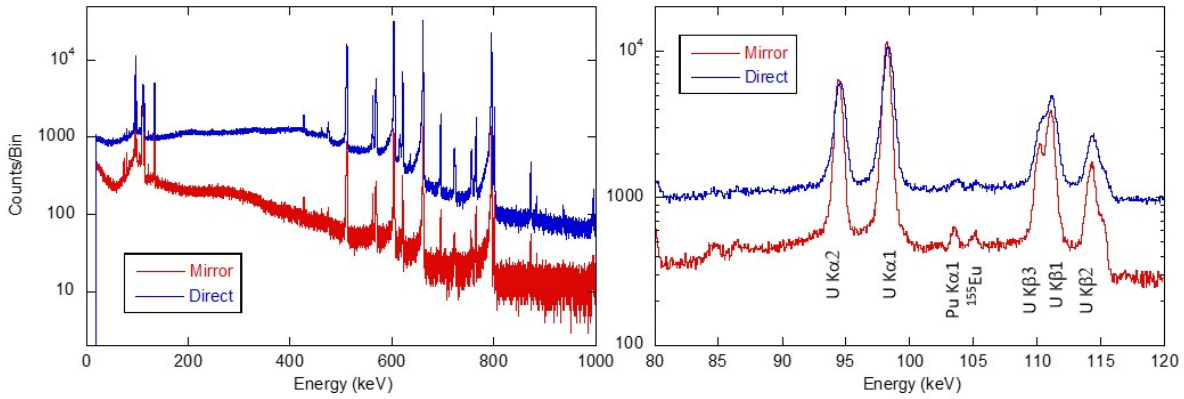

Fig. 1. Equal-time spectra of Rod A at position x/L=0.26 with (red) and without (blue) the gamma-ray mirror. The mirror measurement had a deadtime of 3.7%, while the direct beam measurement has a deadtime of 54.1%.

Recently, we demonstrated the use of gamma-ray mirrors to act as a spectral band-pass filter to facilitate such measurements [2, 3]. The mirrors are manufactured by depositing many bi-layer pairs of SiC/WC onto flat surfaces and the alternating indices of refraction of the materials enhance shallow angle reflection from the surfaces via Bragg reflection [4, 5]. While the maximum reflection angle is relatively small (~ 0.2°), the reflection efficiency can be quite high (~90%), and over distances of several meters the reflected beam can be completely separated from the direct beam, allowing a detector to only see the reflected radiation. This enables the use of high-resolution HPGe spectrometers to perform NDA measurements with no concerns about event rate; a capability demonstrated with fuel as young as seven months since discharge [6].

While the previous work demonstrated the overall concept, that work used a gamma-ray mirror based on a single multi-layer pair spacing of 1.5 nm and a mechanically cooled, position-sensitive, HPGe detector (~ 2 keV FWHM resolution) [7] chosen to allow visualizing the deflected beam, to facilitate understanding the mirror performance. While this allowed quantitative results by comparing the relative intensities of the prominent U Kα and Kβ lines, at best we were able to document the presence of the Pu/Eu line complex and that its width was commensurate with the presence of the Pu Kα emission.

More recently, a new mirror was fabricated, specifically optimized for these measurements by applying a variable spacing to the multi-layer deposition [8]. With the single bi-layer pair spacing the energy-angle relationship of the Bragg reflection is quite narrow so that the mirror only passes radiation from a small portion of the fuel to the detector. The net reflectivity of the system is enhanced if collimation before the mirror is limited, allowing different locations on the rod to meet the reflection criteria, but that also increases the background at the detector due to shallow angle scatters in the mirror system. With a variable spacing multi-layer, the energy-angle relationship is broadened so that a broader spectral range from a larger region of the fuel pin reaches the detector. The new mirrors used a coating design comprising 437 bi-layer pairs to produce a flat-top spectral response over a bandpass from 94-110 keV with a reflection angle of ~ 0.2^0 (Fig. 2) for a ~ 5-fold increase in flux at the detector. In addition to improving the coating, the length of the mirrors was also increased to increase the amount of flux intercepted, and a two-mirror stack was used. Overall, we measured an order of magnitude increase in flux as compared to a single flat mirror with the uniform coating. The results reported below were collected with the optimized 2-mirror optic.

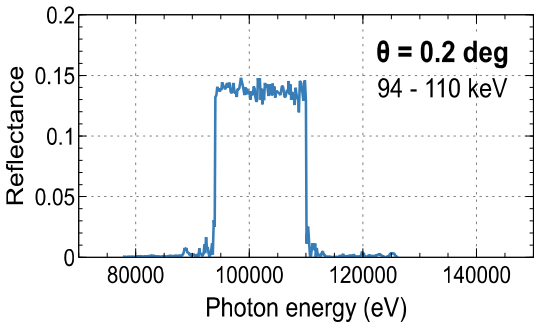

Fig. 2. Theoretical reflectivity curve of the optimized mirrors at a graze angle of 0.2°.

Experimental Approach

Measurements were performed at the Oak Ridge National Laboratory (ORNL) Irradiated Fuel Examination Laboratory (IFEL). IFEL contains hot cells capable of handling full-length spent fuel pins, and includes ports through the concrete walls that allow radiation from the pins to reach the immediately adjacent, shirt-sleeve-environment laboratory where the measurements were performed (Fig. 3). The experiment was installed in one such port that sits in front of a motorized fuel pin translation system that allows one to look at different axial locations on a fuel pin. At the hot cell end of the port, a 2-mm-thick, 75-mm-diameter, sapphire window is used to keep contamination from the cell from reaching the laboratory and serves as a radiation window. This closes the end of the 10-cm diameter port that was filled with a segmented coarse lead collimator used in the previous measurements [3]. The collimator is 109 cm long and has a rectangular beam channel that is 6.98 cm wide by 0.5 cm^2 high. The fuel pin was an additional 20 cm beyond the end window. The inside surfaces of the collimator were painted with silver paint to reduce lead K-shell fluorescence. The gamma-ray mirror mount/manipulator system was installed at the port exit from the hot-cell wall. It includes positions for up to three mirrors, and provides precise multi-axis, computer-controlled motion of the mirrors, which are mounted horizontally with the reflecting surface oriented toward the ceiling (Fig. 3).

Immediately in front of the mirrors is a location for installing additional collimation used to reduce the height of the radiation beam to that needed to fully expose the length of the mirrors. With a 0.2^0

reflection angle and a mirror length of 26 cm, this means a height of 1 mm for a single mirror. For the measurements reported here, a two mirror 'stack' was used that had a mirror spacing of 1 mm so that the optimum beam height was 3.0 mm. The collimation was formed using two machined W blocks with a thickness to the beam of 5 cm with the beam height defined using spacers between them.

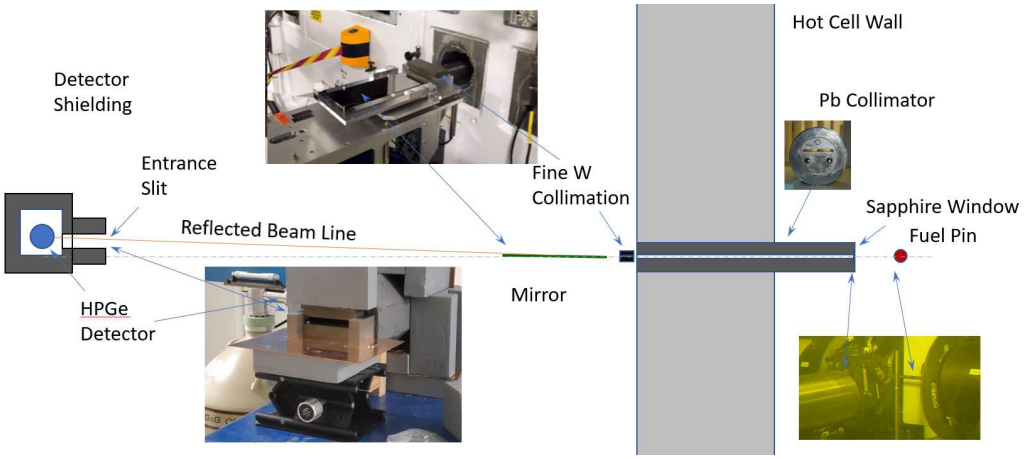

Fig. 3. Schematic of the Experimental layout and photographs of the setup.

To allow maximum separation of the reflected and direct radiation beams from the mirror, the detector was installed 3.6 m from the mirrors at the laboratory's far wall from the port. This allowed translation of the reflected beam 3 cm from the primary beam, with lead/W blocks used as the primary beam stop. In the previous work, room flux was a significant contributor to the detector background so in these measurements the detector was placed in a shielded enclosure constructed primarily from lead bricks and including internal layers of graded-Z shielding with Tin and Cu sheets. Radiation reaching the detector was admitted by a coarse slit defined by two lead bricks separated by spacers to define the desired beam height. The bricks were placed on a heavy-duty lab jack so that the height of the slit could be adjusted to allow either the direct or the reflected beam to reach the detector. In addition, the entire shielding/detector assembly was located on a table with adjustable height to facilitate alignment.

Alignment

Initial beam line

With the small reflection angles and long distances associated with the measurement, precise alignment was crucial. However, once aligned, the system was stable for the week-long measurement campaign. At the heart of the alignment is the radiation beam formed by the fine W collimation immediately in front of the mirrors and its relationship to the 'distant' fuel pin inside the hot cell. Ideally the beam originates at the center of the pin where shielding by the cladding is minimized. To form this beam, a multi-step alignment was used. First, a coarse beam line was established by using a laser located in the lab between the mirror and detector locations. The laser could be rotated through 180^0 to continue the beam line from the hot-cell direction to that of the detector. It was brought into alignment with the long lead collimator in the hot cell wall by iteratively adjusting the height and angle of the beam to the centers of the collimator at the laboratory wall and the fuel pin. The beam location inside the hot cell was observed through a hot cell window next to the port location and using a dummy fuel pin placed in the translator. Final laser alignment was made by auto-collimation of the reflected beam off the sapphire window, e.g. having it return to the center of the laser while maintaining the beam at the collimator and pin centers.

Once adjusted, the laser served as the coarse beam line to which the mirrors and lower tungsten collimator block were aligned using the mirror positioning actuators so that they were parallel to and on the centerline of the laser beam. The laser was also rotated to the detector-side of the lab and the detector height set for a position-sensitive HPGe detector. This concluded the initial system alignment.

Fine alignment

Fine alignment was achieved using radiation from a spent fuel pin. For this stage of the process, the laser was removed and the fine tungsten collimation was established by placing the upper tungsten block (which was not used for the laser alignment) on the lower one with 250 micron spacers to define the location of the radiation beam that would be used for the measurements. The first step was to optimize the collimation alignment with the fuel pin location so that the pitch (angle with respect to the beamline) of the collimator was adjusted to maximize the radiation reaching the detector. A similar optimization was performed in yaw (angle perpendicular to the beamline). Finally, the vertical location of the collimator was also adjusted. With those measurements complete, the tungsten collimator now defined the beam that would hit the mirrors.

Mirror alignment was performed similarly to that of the tungsten collimator. First the mirror was raised in height until it fully blocked the beam. It was then lowered to the center of the beam and its pitch adjusted to maximize the flux (to set the zero angle of the mirror). Finally, the yaw was adjusted. Once aligned in angle, a final height scan was performed so the mirror surface was brought in line with the bottom of the radiation beam.

With those alignments complete, the graze angle of the mirror was changed (with an actuator that raises the back end of the mirror), and the deflected beam observed with the position-sensitive HPGe detector. The W/Pb blocks forming the bottom of the detector entrance slit were raised so that the direct beam was blocked or just barely visible on the position-sensitive HPGe detector. The detector height was set so the reflected beam would be near the center line of the detector to maximize the width of the measured reflected beam and the fine collimation set to 3 mm. A 'rocking-curve' (Fig. 4) was generated for the mirror by progressively increasing its angle with respect to the beam, while the intensity of the U K-shell radiation was observed. Finally, the lower W block of the detector entrance slit was adjusted to fully block the direct beam and the upper W block was positioned using different spacers. The final spacer height was selected so that the counts observed by the detector were not impacted by the upper block. This defined the mirror configuration.

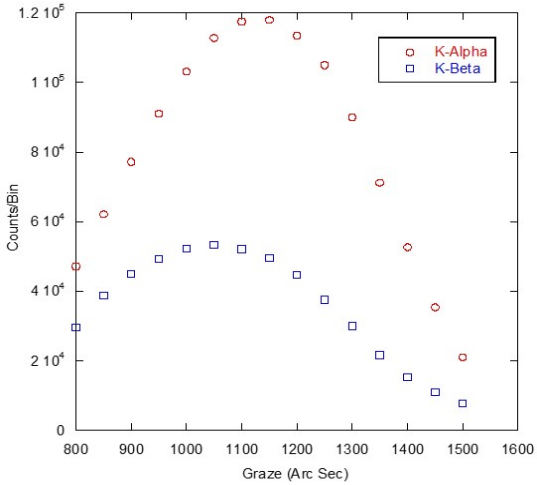

Fig. 4. Rocking curves obtained from the 2-mirror configuration. The spectral bands were 91.5-101 keV and 107-117 keV for the Kα and Kβ plots, respectively.

For direct beam measurements, the mirror was moved out of the beam and the height of the tungsten collimation reconfigured from 3 mm to 250 μm, to control the direct flux reaching the detector. The detector entrance slit was reconfigured to a total height of 3.8 cm with the upper edge (now defined by a Pb brick) at the same location with respect to the detector, lowering the bottom edge to allow the direct beam to reach the detector.

With the optical alignment complete, the position-sensitive HPGe was replaced with an inverted, coaxial point contact p-type HPGe detector oriented so that the beam entered through the diameter of the detector's cylindrical surface.

Measurements

Measurements were made on 3 fuel pins (Table 1). At each location, data were collected in three configurations: the reflected beam with the mirror at the peak of the rocking curve (1100"), a background with the mirror angle moved off resonance to 2500", and a direct beam measurement with the mirror lowered out of the beam and the collimation reconfigured as described above.

Table 1: Fuel Pin Information

Identifier	Burnup MWd/KgU	Discharge Date	Measurement Location (fraction of rod length) x/L			
A	30.4	Oct 2020	.07	0.26	0.75	
B	73.8	Sep 2011		0.26	0.75	
C	17	Feb 2020				0.11

Data were collected from the coaxial detector using an Ortec Digidart [9] to control the instrument and integrate the spectra. The detector parameters were set to a rise time of 10 and a flattop time of 2, giving a full width at half maximum (FWHM) energy resolution of ~ 650 eV, which was determined by fitting the U Kα1 peak in each spectrum to a Gaussian profile. Sample spectra collected from the fuel pins are presented in Fig. 5. Data were collected under computer control with individual run integration times typically set to an hour and the total number of runs for a given configuration set by flux rates and personnel schedules (direct beam measurements were typically taken during the day and mirror measurements taken overnight).

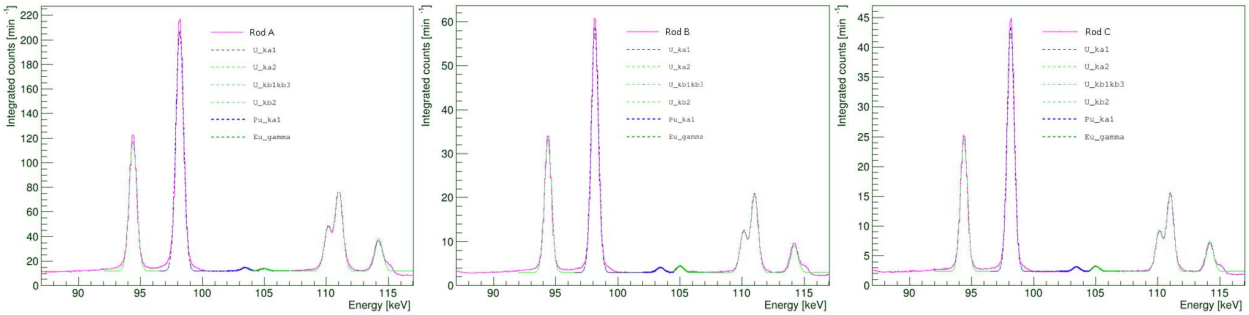

Fig. 5. From left to right, spectra from the x/L=0.26 location of Rods A, B, and at x/L=0.11 for Rod C, respectively. The spectra also show the Gaussian fits to the various peaks.

In addition to the fuel pin measurements, we collected data to determine the dead-layer thickness in our p-type HPGe detector. The outer contact of the detector was made using a diffused layer of Li and the thickness of that layer increases due to further diffusion when the detector is warm, and can result in a dead region up to 1 mm thick. The measurements were performed with a 14.8 MBq ^{133}Ba source set ~ 2 m from the detector. A rectangular beam 2 mm high incident on the diameter of the long axis of the cylindrical detector to mimic the beam reaching the detector from the mirrors in the fuel pin measurements was defined at the detector by the same W blocks used as fine collimation before the mirrors.

Analysis

As fluorescence lines, the absolute flux generated in each of the measured lines is a function of the local radiation environment that excites the atoms and this is assumed to be the same for the U and Pu in the fuel pin. The relative intensities (at the emission site) are given by the elemental abundances (assuming equal excitation cross sections for U and Pu) and the deexcitation branching ratios. The latter terms are

known and for U and can be used to validate the overall results by comparing the different line intensities (e.g. U Kα2/Kα1 and Kβ2/Kβ1). With equal excitation and deexcitation probabilities, one can determine the elemental ratio of U to Pu by taking the ratio U Kα1/Pu Kα1.

Table 2: Spectral Regions of Interest

Energy (keV)	Source	Line
93-96.5	U	Kα2
97-100.5	U	Kα1
103-104.6	Pu	Kα1
104.6-106.2	^{155}Eu	nuclear
109-113	U	$K\beta_1$ and $K\beta_3$
113-117	U	$K\beta_2$

To determine the Pu:U ratio, data from each run were corrected for livetime to obtain a count rate. Background was subtracted from the different spectral windows used (Table 2) and then the flux in each spectral region of interest (ROI) determined by integration. Finally, each number was corrected for attenuation based on the known line energy. Each of these steps is explained in greater detail below. Although the primary concern for the measurements were for the U Kα1 and Pu Kα1 lines, we also include the results of the U Kα2 and Kβ lines as a comparison to check for systematic shifts in the results. Table 2 also includes the other lines observed in the mirror band pass.

Background

Two types of background were considered. First, flux reaching the detector with the mirror out of resonance (angle of 2500") but with each rod in place. Second, the background under each peak from the flux that reaches the detector in either the direct or reflected configurations. In both cases the background was observed to be constant over the overall energy region of interest. The out-of-resonance background, was found to contribute only a small amount to the background with beam on the detector, so in the end, both backgrounds were handle in a single step. Specifically, the peak-free ROI from 101-to-103 keV was used to determine the average background per spectral bin.

Integration

Simple integration of the different regions of interest (ROI) associated with each peak was used to determine the net counts in a peak. Before integration, the background defined above, was subtracted from each spectral bin of the data. The results of the analysis are given in Table 3 (after correction for differential attenuation).

Table 3: Measurement Results

Rod	Location x/L	U Kα1	Pu Kα1	Ratio Pu/U	Uncert.	U Kα2	Rat U α2/ α1	Uncert.	U Kβ1,3	Rat U β1,3/ α1	Uncert.
A	0.07	1999.09	18.07	0.904	0.008	1316.20	65.84	0.00090	614.67	30.75	0.00030
	0.26	3051.76	29.07	0.953	0.010	2002.31	65.61	0.0011	983.83	32.24	0.00038
	0.75	2563.78	25.65	1.000	0.014	1683.66	65.67	0.0016	785.35	30.63	0.00052
B	0.26	799.86	11.94	1.493	0.008	525.44	65.69	0.0007	243.49	30.44	0.00024
	0.75	808.15	12.02	1.488	0.031	523.66	64.80	0.0028	249.10	30.84	0.00094
C	0.26	585.81	7.99	1.364	0.017	383.34	65.43	0.0016	177.28	30.26	0.00053

Differential Attenuation Corrections

The measured values for each of the line intensities are impacted by attenuation through overlying materials, including self-attenuation in the fuel, the cladding, the atmosphere, the detector housing and the detector dead layer. Because any two lines used to form the final ratios are at slightly different energies, it is important to correct for differential attenuation in each of these materials. The corrections normalized to the Kα1 line attenuation are given in Table 5, and described in more detail below. Note that those values are applied at the known energy of each of the lines, which are narrow compared to the

detector resolution. The correction for the Kβ lines is weighted based on the expected relative line intensities for a net correction of 0.631 for the total counts in the ROI.

Table 3: Differential Attenuation Corrections

	U Kα2	U Kα1	Pu Kα1	U Kβ3	U Kβ1
Energy (keV)	**94.66**	**98.44**	**103.7**	**110.4**	**111.3**
Air	1.002	1.000	0.998	0.995	0.995
2 mm Sapphire	1.003	1.000	0.997	0.993	0.993
HPGe Detector	1.008	1.000	0.993	0.988	0.988
Cladding	1.054	1.000	0.940	0.867	0.865
Fuel	1.099	1.000	0.879	0.755	0.742
Net	**1.170**	**1.000**	**0.816**	**0.640**	**0.626**

Sapphire window and air

The effects of the Sapphire window and passage through air are estimated using XCom attenuation cross-sections [10] at the line energies, and the path lengths through each material. The cross-sections that include coherent scatter are used since such scatters still deflect radiation and keep it from reaching the detector.

HPGe

To determine the dead layer of the HPGe detector, the 53-keV and 81-keV lines from the collimated ^{133}Ba-source data described above were used together with Monte Carlo simulations. To obtain the intensities of the two spectral lines, the counts were extracted using a least-squares fitting routine implemented in the Geant4, Root analysis platform. A Gaussian form was used for the 53-keV peak with a step function centered at the location of the peak for the background. For the 80-keV region, Gaussian functions were used for the peaks at 80- and 81-keV above a background fitted by a step function at the centroid of the 81-keV peak.

Simulations with different dead-layer thicknesses were then performed using the Monte Carlo radiation transport toolkit Geant4. The simulations included the stainless-steel encapsulation of the source and the internal components of the detector cryostat and crystal using information supplied by the vendors. In the simulations, collimated primary gamma rays at each of the known peak energies were thrown into a rectangle along the side of the detector to match the geometry from the measurement. The number of full-energy depositions were recorded and the best match to the measured data as a function of the dead-layer thickness were determined. This gave a value of 565 μm, which was then used to generate a detector response curve (Fig. 6) by simulating the response at 1 keV intervals. Those values were fit by a fourth order polynomial to obtain the corrections at each of the line energies. The correction includes the Al cryostat housing.

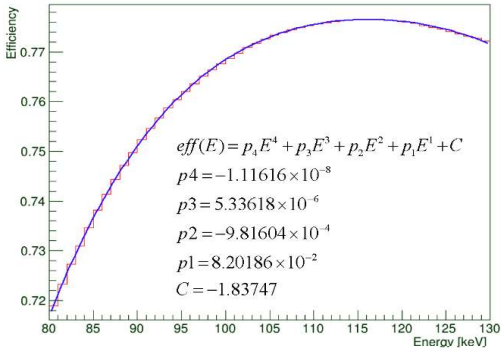

Fig. 6. Final efficiency curve used for the HPGe

Fuel and Cladding

The effects of attenuation from the fuel itself and the cladding are more complicated than can be determined using simple attenuation through a thickness of material as used above. The fuel has different skin depths for the different emission lines, so that compared to the local emission, more radiation at higher energies reaches the fuel's surface. The cladding has a relatively tight radius so that emission from different locations will have to traverse different cladding thicknesses, depending on that location. To handle this, a Monte Carlo model in MCNP6.3.0 [11] was used to determine these effects. It assumed fuel uniformly distributed in an 8-cm-long fuel pin segment. Two cases were run, one that launched x-rays with the theoretical relative intensities of the U K-shell fluorescence lines, and a second

that launched the Kα1 lines from U and Pu with equal intensities. The relative intensities of the radiation leaving the fuel and the cladding were tallied and used to create the correction factors in Table 3. Note that these are the dominant overall corrections.

Discussion

The expected Pu:U ratios from neutronic burnup-depletion simulations of the fuel pins performed in ORIGEN [12] are compared to the measurements for the various rods and locations in Table 5. It is immediately obvious that the values differ significantly, and this is not surprising because the expected values are for the full volume of a rod at any axial location, while the limited range of the K-shell x-rays (Mean free path ~ 500 μm) means that the measured values probe only the outer surfaces of the rods. It has been well documented [1,13] that fission occurs preferentially in the outer regions of a fuel pin so the x-ray measurements should expect to see more Pu because it preferentially grows in at the pin surface. This accounts for the systematic bias between the measured and the expected values.

Table 4: Results

Rod	Location	Expected Pu (Wt%)	Measured (%)
A	0.07	0.46	0.904
	0.26	0.67	0.953
	0.75	0.67	1.000
B	0.26	0.97	1.493
	0.75	0.97	1.488
C	0.26	0.54	1.364

The A and B rods were used in similar reactors so that their primary difference is that the latter has almost twice the burnup of the former, and the measurements show that as a ~ 1:1.5 change in the ratio of the Pu content. This actually agrees fairly well with the ratio of the expected values which normalize to 1:1.45. These results are in good agreement despite the much younger age of Rod A. In fact in the direct measurements, with the much smaller slit height, Rod A had deadtimes as high as 50%. Typical deadtimes for the measurements using the mirror were negligible at ~ 2%.

The rods were also evaluated at different axial locations defined by the fraction of a location, x, to the total rod length, L. Measurements were performed in the enriched peak-power producing regions of the fuel rod (x/L 0.26 and 0.75) to see if there were significant differences in Pu content as a function of position. While the B rod does not show a statistically significant difference, Rod A shows a 5% lower Pu:U ratio at x/L = 0.75 than at x/L = 0.26. What is unexpected is that in the depleted section of fuel stack where neutron fluence is lower (rod A at x/L = 0.07), the measured Pu content is only down to 93% of the average found in the power producing section of the rod, while it is expected to be down to 69%. The source of this discrepancy is not known.

The shortest mirror measurement was three hours long and achieved a Pu:U ratio of 1.49% with a statistical uncertainty of ± 0.03% on the quieter B rod. This indicates that in one tenth the time (~ 20 min) one could achieve a useful precision of ± 0.1%. A time that could be reduced further with parallel measurements indicating that practical evaluation of Pu content on some fraction of the fuel pins in an assembly could be achieved in real time.

To be of value, one must understand the systematics of the measurements, and here some work remains. There are the obvious issues associated with the fact that the measurements probe the Pu-enriched outer surface of the fuel pin and these need to be related to the net Pu content locally integrated over the whole pin volume. In this regard the favorable comparison of the Rod A and B normalized ratios are encouraging. However, the unexpectedly high Pu content of the depleted region of Pin A is puzzling.

There are also systematic issues raised when we compare the theoretical ratios of the different U lines (Kα2/Kα1 at 61.79%, and Kβ1,3/Kα1 at 35.6%) to the measured values of 65.4% and 30.9%, respectively. The low value of the latter can be partially explained by the fact that the higher energies of the Kβ lines means that they originate from deeper into the fuel pin, and just as the Pu content falls off, we expect the concentration of other fission by products to fall off as well. Hence the deeper layers of the U will present a quieter radiation environment, so the fluorescence will not be as strong. To better understand this would require a more elaborate simulation that includes non-uniform excitation of the emission when trying to account for self-attenuation in the fuel. It is possible that this same effect also occurs to a lesser extend when comparing the Kα2/Kα1 ratio, noting that here radial effects will lead to higher ratios.

Conclusion

The measurements demonstrate that gamma-ray mirrors provide a means of performing non-destructive analysis on spent nuclear fuel pins without the need for specialized high rate detectors and that such measurements can be conducted in well under an hour. The results are consistent in that the ratios of the U-only lines are tightly grouped, as are the different U:Pu ratios at different locations along the A and B rods. The unexpectedly high Pu content in the lowest x/L location measured in the ^{238}U region of the A rod is a mystery.

References

1. W.S. Charlton, et al. "The Use of Self-Induced XRF to Quantify the Pu Content of PWR Spent Nuclear Fuel," presented at 31st ESARDA Annual Meeting, Vilnius, Lithuania, May 26–28, 2009, Available: http://nsspi.tamu.edu/wp-connection/upload-links/p19_pub2.pdf.
2. K.P. Ziock, et al "U and Pu gamma-ray measurements of spent fuel using gamma-ray mirror band-pass filter," in IAEA Symposium on International Safewards, IAEA-CN-220 (2014)
3. J. Ruz, et al., "Direct measurement of ^{235}U in spent fuel rods with gamma-ray mirrors," Nucl. Instrum. Meth. Phys. Res. Sect. A 777, 15–19, 2015.
4. M.J. Pivovaroff et al., "Gamma-ray mirrors for direct measurement of spent nuclear fuel," Nicl. Inst. Meth. Phys. Res., **A743**, 109-113, 2014.
5. M. Fernandez_Perea, et al. "Physics of reflective optics for the soft gamma-ray photon energy range," Phys. Rev. Lett. 111:027404, 2013.
6. J. Ruz, et al. in preparation for submission to Nucl. Inst. Meth. in Phys. Res.
7. GeGI detector, PHDS, Inc., 3100 Amherst Rd. Knoxville, TN 37921.
8. C. Burcklen, et al. "Aperiodic x-ray multilayer interference coatings with high reflectance and large field of view," Proc. SPIE 10619, 10691OU, 2018.
9. AMETEK/ORTEC, 801 S Illinois Ave, Oak Ridge, TN 37830.
10. M.J. Berger, et al., XCOM: Photon Cross Sections Database, https://dx.doi.org/10.18434/T48G6X
11. M.E. Rising, et al., MCNP Code Version 6.3.0 Release Notes, Los Alamos National Laboratory, Tech. Rep. LA-UR-22-33103, Rev. 1., Los Alamos, NM, USA, January, 2023.
12. W.A. Wiselquist, "The Scale 6.2 ORIGEN API for High Performance Depletion," Joint Int. Conf. on Math. And Comp. (M&C, Supercomp. In Nucl. App. (SNA) and the Monte Carlo (MC) Method," Nashville, TN, 2015, www.ornl.gov/sites/default/files/2015_ORIGEN_API_paper_146_1.pdf.
13. C.T. Walker, et al., "SIMS analysis of an UO_2 fuel irradiated at low temperature to 65 MWd/KgHM," J. Nucl. Mater., **393**, 212-223, 2009, doi.org/https://doi.org/10.1016/j.jnucmat. 2009.06.017.